Progress in Scientific Computing, Vol. 6
Proceedings of U.S.-Israel Workshop, 1984

Secondary Instability of Free Shear Flows

Marc E. Brachet[1], Ralph W. Metcalfe[2], Steven A. Orszag[3], James J. Riley[4]

Abstract

The three-dimensional stability of saturated two-dimensional vortical states of planar mixing layers and jets is studied by direct integration of the Navier-Stokes equations. Small-scale instabilities are shown to exist for spanwise scales at which classical linear modes are stable. These modes grow on convective time scales, extract their energy from the mean flow, and persist to moderately low Reynolds numbers. Their growth rates are comparable to the most rapidly growing inviscid instability and to the growth rates of two-dimensional subharmonic (pairing) modes. The three-dimensional modes do not appear to saturate in quasi-steady states. Indeed, they seem to lead directly to chaos. Results are presented for the resulting three-dimensional turbulent states.

[1] CNRS, Observatoire de Nice, 06-Nice, France
[2] Flow Research, Inc. Kent, WA 98032
[3] Princeton University, Princeton, NJ 08544
[4] University of Washington, Seattle, WA 98105

1. Introduction

Free shear flows like those of mixing layers and jets differ from wall-bounded flows in the sense that they are typically inflexional and, hence, are subject to inviscid instabilities. Thus, it may be thought that the process of transition to turbulence in free-shear flows would be inherently simple and amenable to analysis. Indeed, observations by Winant & Browand (1974), Brown & Roshko (1974), Wygnanski et al (1979), Ho & Huang (1982), Hussain (1984), and others show the central role played by two-dimensional dynamical processes through transitional regimes in these flows. While three-dimensional small scales are observed (Miksad 1972, Bernal et al 1979), they may not destroy the large-scale two-dimensional structure (Browand & Troutt 1980). In contrast, studies of wall-bounded flows have emphasized the central role of three-dimensional effects in their breakdown to turbulence.

In this paper, we investigate the nature of linear instabilities of saturated nonlinear two-dimensional flow states that arise from the primary inviscid instability of free shear flows. It is shown that these saturated two-dimensional states are subject to a class of strongly unstable three-dimensional modes that are present even at moderately low Reynolds numbers. It is possible that these three-dimensional instabilities can explain some of the initial stages of three-dimensional transition in free-shear flows. We find that the two-or three-dimensional character of these free-shear flows depend crucially on initial conditions as there is a close competition between the various modes of instability to be discussed below.

The approach followed here is similar to that used by Orszag & Patera (1980, 1981, 1983) in studies of secondary instabilities in wall-bounded flows. The parallel laminar flow is perturbed initially by a finite-amplitude two-dimensional disturbance that is allowed to evolve and to saturate in a quasi-steady state. The stability of this finite amplitude vortical state to both subharmonic (pairing) two-dimensional modes and smaller-scale three-dimensional modes is then studied by numerical solution of the full three-dimensional time-dependent Navier-Stokes equations. The character of the pairing instability was first explained theoretically by Kelly (1967) and numerically by Patnaik, Sherman & Corcos (1974) and Collins (1982) for stratified flows and by Riley & Metcalfe (1980) and Pierrehumbert & Widnall (1982) for unstratified flows; the present results confirm the strength of this kind of mode.

Pierrehumbert & Widnall (1982) have made a study of the linear two- and three-dimensional instabilities of a spatially periodic inviscid shear layer that is closely related to the present study. They consider the stability characteristics of the model family of two-dimensional vortex-modified mixing layers with velocity fields

$$\begin{aligned} u &= \sinh z \,/(\cosh z - \rho \cos x) \\ w &= -\rho \sin x/(\cosh z - \rho \cos x) \end{aligned} \tag{1.1}$$

(Stuart 1967) for $0 \leq \rho < 1^{+}$ and study subharmonic pairing instabilities and a new 'translative' three-dimensional instability. In contrast, we consider here both the linear and nonlinear stability characteristics of time-developing viscous shear layers. The three-dimensional secondary instability studied here is both the analog of the translative instability and the generalization of the instability analyzed by Orszag & Patera for wall-bounded flows.

$^{+}$ Note that for $\rho \ll 1$, the basic flow state (1.1) is of the form $\tanh z\, \hat{x} + \rho \mathrm{Re}[e^{ix}\underset{\sim}{v}(z)]$. This flow state is an inviscidly neutrally stable perturbation of the mixing layer $\tanh z\, \hat{x}$. At wavenumber 1, there are no primary two-dimensional instabilities that can compete with the subharmonic and secondary instabilities. In contrast, the results to be reported in Section 3 involve unstable primary perturbations to the mixing layer.

2. Numerical Methods

The Navier-Stokes equations are solved in the form

$$\frac{\partial \vec{v}}{\partial t} = \vec{v} \times \vec{\omega} - \nabla \pi + \nu \nabla^2 \vec{v} \tag{2.1}$$

$$\nabla \cdot \vec{v} = 0 \tag{2.2}$$

where $\vec{\omega} = \nabla \times \vec{v}$ is the vorticity and $\pi = p + 1/2\ v^2$ is the pressure head.
Periodic boundary conditions are applied in the streamwise, x, and spanwise, y, directions,

$$\vec{v}(x + \frac{4\pi}{\alpha}, y, z, t) = \vec{v}\ (x,y,z,t), \tag{2.3}$$

$$\vec{v}(x,y + 2\pi/\beta, z, t) = \vec{v}(x,y,z,t)$$

while the flow is assumed quiescent ($v \to U_{\pm} \hat{x}$, $U_{\pm}$ constants) as $z \to \pm \infty$. Note that the assumed periodicity length is $4\pi/\alpha$ to accommodate both the primary mode with x-wavenumber α and its subharmonic with x-wavenumber $\frac{1}{2}\alpha$+.

\+ Pierrehumbert & Widnall (1982) point out that Floquet theory implies that the Navier-Stokes equations linearized about a flow periodic mix admit solutions of the more general form $v(x,y,z) = e^{i\gamma x}\ \bar{v}(x,y,z)$ where $\bar{v}$ is periodic in x with the same periodicity as the basic flow and γ is arbitrary. However, Pierrehumbert & Widnall consider only the subharmonic and primary cases. The analysis, which has not yet been done for more general γ, may yield important new results. Indeed, Busse (1979) points out the importance of these general γ modes in Benard convection. The present study is restricted to γ being a half-integer multiple of the primary wavenumber because our code is fully nonlinear with the periodicity condition (2.3).

The assumption of periodicity in the streamwise-x direction is unrealistic in a spatially growing mixing layer unless the modes being studied are localized in x and grow much more rapidly than the shear layer spreads. These latter approximations seem reasonably well justified for the three-dimensional modes studied here (see Sec. 3). However, future work using inflow-outflow boundary conditions in x should clarify the role of non-parallel effects in free-shear flows.

The dynamical equations are solved using pseudospectral methods in which the flow variables are expanded in the series

$$\vec{v}(x,y,z,t) = \sum_{|m|<\frac{1}{2}M} \; \sum_{|n|<\frac{1}{2}N} \; \sum_{p=0}^{P} \vec{u}(m,n,p,t)\, e^{im\alpha x} e^{in\beta y} T_p(Z) \tag{2.4}$$

where n and p are integers and m is a *half-integer* when pairing is allowed and a whole integer if pairing is excluded. Here $Z = f(z)$ is a transformed z-coordinate satisfying $Z = \pm 1$ when $z = \pm \infty$. Two choices of $f(z)$ have been studied, viz.

$$Z = \tanh \frac{z}{L} \quad (|z|<\infty, \; |Z| < 1) \tag{2.5}$$

and

$$Z = \frac{z}{\sqrt{z^2 + L^2}} \quad (|z|<\infty, \; |Z| < 1) \tag{2.6}$$

where L is a suitable scale factor. With these mappings, derivatives with respect to z are evaluated pseudospectrally using the relations

$$\frac{\partial \vec{v}}{\partial z} = \frac{1}{L} (1 - Z^2) \frac{\partial \vec{v}}{\partial Z} \tag{2.7}$$

$$\frac{\partial \vec{v}}{\partial z} = \frac{1}{L} \sqrt{1 - Z^2} \quad \frac{\partial \vec{v}}{\partial Z} \tag{2.8}$$

for (2.5), (2.6), respectively.

Time stepping is done by a fractional step method in which the nonlinear terms are marched in time using a second-order

Adams-Bashforth scheme while pressure head and viscous effects are imposed implicitly using Crank-Nicolson differencing.

This scheme is globally second-order accurate in time, despite time splitting (Deville & Orszag 1983), because the various split operators commute in the case of quiescent boundary conditions at $z = \pm\infty$.

There is one further technical detail regarding the numerical method that should be discussed here. Various Poisson equations, like

$$\frac{d^2\Pi}{dz^2} - (m^2 + n^2)\Pi = g(z) \qquad (|z|<\infty) \tag{2.9}$$

are solved by expansion in the eigenfunctions of d^2/dz^2:

$$\frac{d^2}{dz^2} e_k(z) = \lambda_k e_k(z) \qquad (|z|<\infty) \tag{2.10}$$

Thus, if

$$g(z) = \sum_{k=0}^{P} g_k e_k(z)$$

Then

$$\Pi(z) = \sum_{k=0}^{P} \frac{g_k}{\lambda_k - (m^2+n^2)} e_k(z) \tag{2.11}$$

We remark that this technique gives spectrally accurate solutions, despite the fact that the continuous version of the eigenvalue problem (2.10) has only a continuous, and hence singular, spectrum. Also, note that all the eigenvalues λ_k are real and non-positive; for both mappings (2.5) and (2.6), there are precisely three zero eigenvalues λ_1, λ_2, λ_3. One of these zero eigenmodes, λ_1, is physical, viz. $e_1(z) = 1$, but the other two are highly oscillatory and unphysical. Indeed, since the spectral (Chebyshev) derivative of $T_P(Z)$ vanishes except at $Z = \pm 1$, $e_2(Z) = T_P(Z)$ is a zero eigenfunction of d^2/dz^2; $T_P(Z_j) = (-1)^j$ at the Chebyshev collocation points $Z_j = \cos \pi j/P$. The third zero eigenmode oscillates and grows roughly like z. When $m = n = 0$, the incompressibility constraint (2.2) requires that this mode of the z-velocity field vanish identically so there is no difficulty with the zero pressure eigenvalues λ_1, λ_2, λ_3.

Comparisons of the behavior of linear Orr-Sommerfeld eigenmodes obtained using the mappings (2.5) and (2.6) show that (2.6) gives a superior representation of these modes unless L is fine tuned, which is not convenient in the nonlinear dynamical runs.[+] Some representative results are given in Table 1. Notice that as α increases, the optimal choice of map scale L decreases. Also, notice that the accuracy of the eigenvalue is much more sensitive to L for the hyperbolic tangent mapping (2.5) than for (2.6).

The nonlinear time-dependent Navier-Stokes code has been tested for the generalized Taylor-Green vortex flow (2.12) and for the behavior of linearized eigenfunctions, with satisfactory agreement being achieved with power series in t (Brachet et al 1983) and linear behavior, respectively.

[+] There is one case in which it seems that the hyperbolic tangent mapping (2.5) is more convenient than the algebraic mapping (2.6). This flow is the generalized Taylor-Green vortex flow that develops from the initial conditions

$$
\begin{aligned}
u(x,y,z,0) &= \sin x \cos y/\cosh^2 z \\
v(x,y,z,0) &= -\cos x \sin y/\cosh^2 z \qquad (2.12) \\
w(x,y,z,0) &= 0
\end{aligned}
$$

The evolution of this flow seems best studied, either by power series or initial value methods, using (2.5) with $L = 1$. The time evolution of this free shear flow is remarkably similar to that of the periodic Taylor-Green vortex (Brachet et al 1983).

Table 1. Growth Rates (Im c) of the Orr-Sommerfeld Eigenfunctions for the Mixing Layer $U_0(z) = \tanh z$ †

x-wavenumber α

	0.25			0.5			0.75		
	Number of Chebyshev Polynomials (P+1)								
L	17	33	65	17	33	65	17	33	65
	Hyperbolic Map (2.5)								
0.5	1.534	1.375	1.238	0.579	0.501	0.457	0.160	0.150	0.150
1	0.959	0.820	0.746	0.383	0.360	0.351	0.141	0.138	0.137
2	0.635	0.614	0.605	0.344	0.342	0.342	0.137	0.137	0.137
4	0.612	0.598	0.597	0.324	0.342	0.342	0.041	0.136	0.137
8	0.539	0.597	0.597	0.115	0.322	0.342	*S*	0.045	0.136
16	0.202	0.526	0.596	*S**	*S*	0.321	*S*	*S*	0.046
	Algebraic Map (2.6)								
0.5	0.699	0.588	0.599	0.345	0.346	0.342	0.131	0.138	0.137
1	0.591	0.599	0.597	0.344	0.342	0.342	0.137	0.137	0.137
2	0.600	0.597	0.597	0.342	0.342	0.342	0.136	0.137	0.137
4	0.597	0.597	0.597	0.325	0.342	0.342	0.371	0.136	0.137
8	0.542	0.597	0.597	0.009	0.322	0.342	*S*	0.043	0.136

† Here the Reynolds number is $1/\nu = 100$ and the eigenvalue is the complex wave speed c for a temporal mode of the form $\psi(z)e^{i\alpha(x-ct)}$. For the most rapidly growing mode listed here, $\mathrm{Re}\ c = 0$.

* *S* indicates that all modes are stable with the indicated parameter values

3. Results for Mixing Layers

In this Section, results are reported for the evolution of initial velocity fields of the form

$$\vec{v}(x,y,z,0) = U_0(z)\,\hat{x} + \mathrm{Re}[A_{10}\vec{v}_{10}(z)e^{i\alpha x} + A_{\frac{1}{2},0}\vec{v}_{\frac{1}{2},0}(z)e^{\frac{1}{2}i\alpha x}$$
$$+ A_{11}\vec{v}_{11}(z)e^{i\alpha x+i\beta y}] \tag{3.1}$$

The laminar mean profile is assumed to be the mixing layer profile $U_0(z) = \tanh z$ and $\vec{v}_{ij}(z)$ is normalized so that $\max|v_{ij}(z)| = 1$. The initial functions $\vec{v}_{ij}(z)$ are normally chosen as the most unstable eigenfunctions of the linear Orr-Sommerfeld equation with the wavenumbers given in (3.1).* In this representation, A_{10} is the amplitude of the primary two-dimensional component, $A_{1/2,\,0}$ is the amplitude of its subharmonic or pairing mode, and A_{11} is the amplitude of the primary three-dimensional wave. In all cases, the initial conditions are chosen so that $A_{1/2,0}\ A_{11} \ll A_{10}$; typically, $A_{10} = 0.25$. Also, the momentum thickness Reynolds number for the undisturbed flow is $R = 1/\nu$.

In the absence of subharmonic and three-dimensional perturbations ($A_{1/2,0} = A_{11} = 0$), the two-dimensionally perturbed flow quickly saturates to a quasi-steady state. In Figure 1, a plot is given of the time evolution of the two-dimensional disturbance energy $E_{10}(t)$ for various initial amplitudes A_{10}.

---

* The Reynolds numbers of the flows discussed below, while modest, are much greater than that of the onset of linear instability ($R_{crit} \approx 4$), so that even the linear modes are effectively inviscid. In this case, damped modes may lie only in the continuous spectrum (Drazin & Reid 1981) and so are singular. Whenever (3.1) calls for such a singular contribution to the initial condition (3.1), we choose instead the flow component $w_{nm} \equiv w_{10}$ of the primary mode (with u_{nm} and v_{nm} determined by incompressibility).

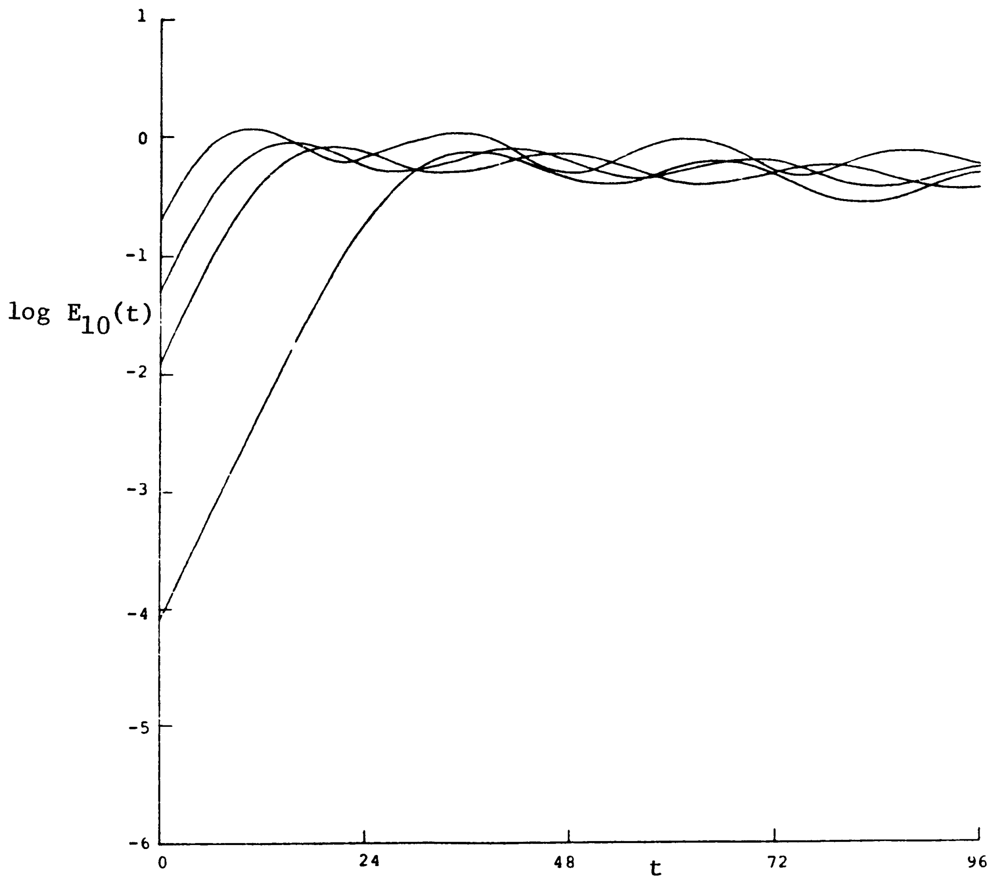

Figure 1.

A plot of $E_{10}(t)$ vs t for runs with $A_{\frac{1}{2},0}$ = A_{11} = 0 and A_{10} = 0.5, 0.25, 0.125, 0.01. Here the Reynolds number is R = 400, $U_0(z)$ = tanh z, the spectral cutoffs in (2.4) are M = 8, N = 1, P = 32, (resolution 8 x 1 x 32 with no pairing modes), the x-wavenumber is α = 0.4, and the time step is Δt = 0.02. Note that the flow saturates into a vortical state nearly independent of the initial perturbation. Before such saturation occurs, the perturbation grows linearly like an Orr-Sommerfeld eigenfunction.

Here

$$E_{mn}(t) = \int_{-\infty}^{\infty} dz \; |\vec{v}_{mn}(z,t)|^{2} \qquad (3.2)$$

where

$$\vec{v}_{mn}(z,t) = \sum_{p=0}^{P} \vec{u}(m,n,p,t)T_{p}(Z) \qquad (3.3)$$

and u is defined by (2.4). It is apparent that E_{10} saturates into a finite-amplitude vortical state on a time scale of order 10; indeed, the mean flow tanh z is inviscidly unstable to the perturbation A_{10} with maximum growth rate roughly 0.2 when $\alpha \approx 0.44$. [The range of inviscidly unstable wavenumbers for the tanh z profile is $0 < \alpha < 1$. Also, note that if we used a length scale in which the wavelength of the perturbation is of order unity (rather than our unity in which the shear layer thickness is order 1), saturation of E_{10} would occur on a time scale of order 1.] In Fig. 2, a plot is given of an instantaneous spanwise vorticity distribution in the developed two-dimensional flow.

Comparison of the energy evolution plotted in Figs. 3(a) and 3(b) shows that the initial phase of the subharmonic perturbation can affect its growth rate but not the eventual growth and saturation of the subharmonic. The present calculations differ from those of Riley & Metcalfe (1980) and Patnaik et al (1976) in that the initial disturbances are chosen to be computationally infinitesimal in our runs in contrast to their finite-amplitude initial perturbations. (Also Patnaik et al study stratified flows). While phase does affect the initial subharmonic growth rate, the perturbation eventually achieves its optimal growth rate during our long time runs. We conclude that the 'vortex shreddy' process found by Patnaik et al is a finite amplitude effect, not reproducable in the present long-time runs.

The saturated two-dimensional flow state discussed above can be unstable to subharmonic perturbations, $A_{1/2,0}$ in (3.1), for suitable α (Kelly 1967). In Figure 3, we plot the evolution of the

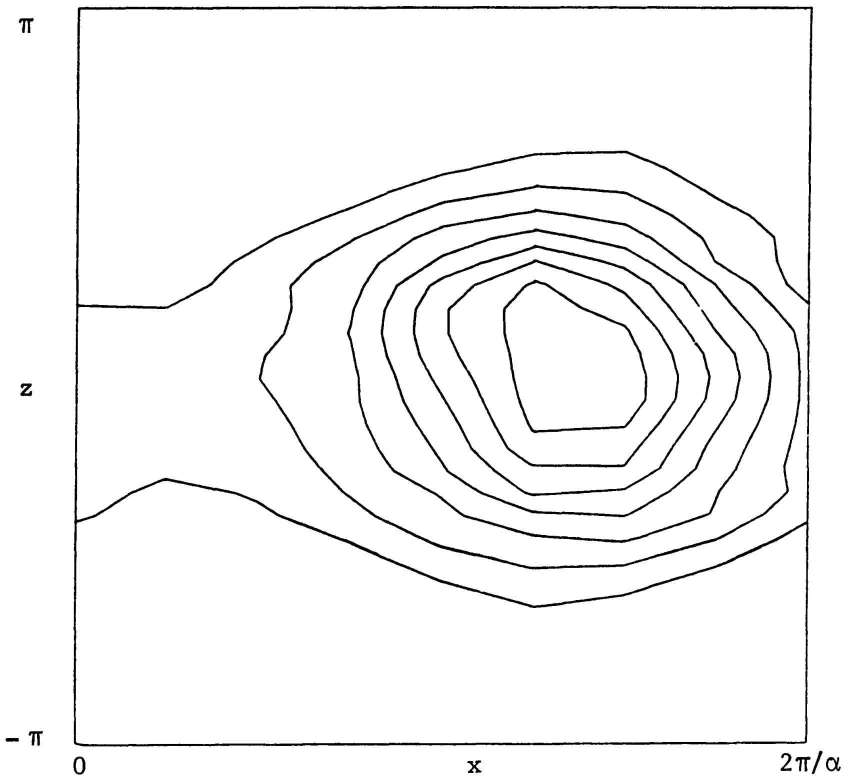

Figure 2.

A contour plot of spanwise (y) vorticity contours for the saturated flow state of the mixing layer at R = 400. The vortex prominent in this plot is nearly stationary.

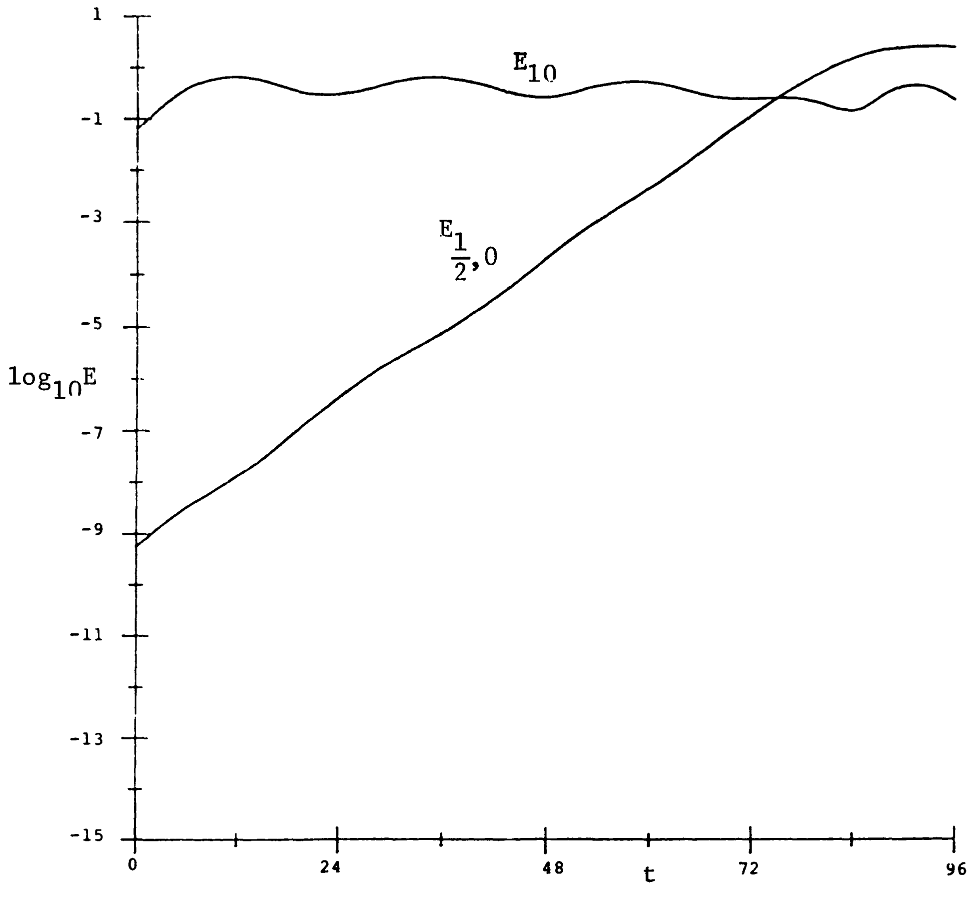

Figure 3.

Plots of the evolution of $E_{10}(t)$ and the two-dimensional pairing mode energy $E_{\frac{1}{2},0}(t)$ as functions of time. Here $R = 400$, $U_0(z) = \tanh z$, $A_{10} = 0.25$, $A_{\frac{1}{2},0} = 3 \times 10 - 4$, $M = 8$, $N = 1$, $P = 32$, (resolution $16 \times 1 \times 32$ with pairing modes) $\alpha = 0.5$ and $\Delta t = 0.02$. (a) and (b) differ by a 90° phase shift of initial subharmonic perturbation.

subharmonic perturbation energies $E_{1/2,0}(t)$ as well as the primary two-dimensional energy $E_{10}(t)$. Here we choose $a_{10} \doteq 0.25$ and $a_{1/2,0} = 3 \times 10^{-4}$. In Figure 3(a), the primary and subharmonic perturbation vorticity are initially in phase; in Figure 3(b) they are initially out of phase. This subharmonic instability of the saturated two-dimensional vortical states is inviscid in character as its growth rate asymptotes to a finite limit as R increases. The growth rate $\sigma_{1/2,0} \approx 0.2$ for $\alpha = 0.8$. These growth rates are not significantly larger than the linear inviscid growth rates of Orr-Sommerfeld modes; however, pairing perturbations are significant because the nonlinear saturation of the two-dimensional Orr-Sommerfeld modes allows the pairing modes to achieve finite amplitudes at later times. The evolution of the spanwise vorticity distribution during pairing instability is revealed by the contour plots given in Fig. 4. The energetics of the pairing instability is revealing. Energetic transfers to and from the pairing mode may be decomposed as

$$\frac{1}{2E_{\frac{1}{2},0}} \cdot \frac{dE_{\frac{1}{2},0}}{dt} \equiv \sigma_{\frac{1}{2},0} = \gamma_M + \gamma_{2-D} + \gamma_\nu \qquad (3.4)$$

where γ_M involves the nonlinear interaction of the pairing mode with the mean flow, γ_{2-D} involves the nonlinear interaction of the pairing mode and all other two-dimensional modes, and γ_ν the viscous dissipation of pairing energy. Here γ_M and γ_{2-D} involve sums over nonlinear terms in the Navier-Stokes equations but are unaffected by pressure; γ_ν is proportional to the enstrophy in the pairing mode. In Fig. 5, a plot is given of these transfer terms as a function of time. It appears that the pairing mode extracts most of its energy from the mean flow and grows no faster than in the absense of the two-dimensional primary component. The important conclusions are that the presence of the saturated two-dimensional primary does not turn off the pairing mode and that the growth rate of this latter mode is of order that observed in the primary two-dimensional instability. These results imply that even a small pairing perturbation will quickly achieve finite amplitude after the primary mode saturates.

While these conclusions are in substantial agreement with those

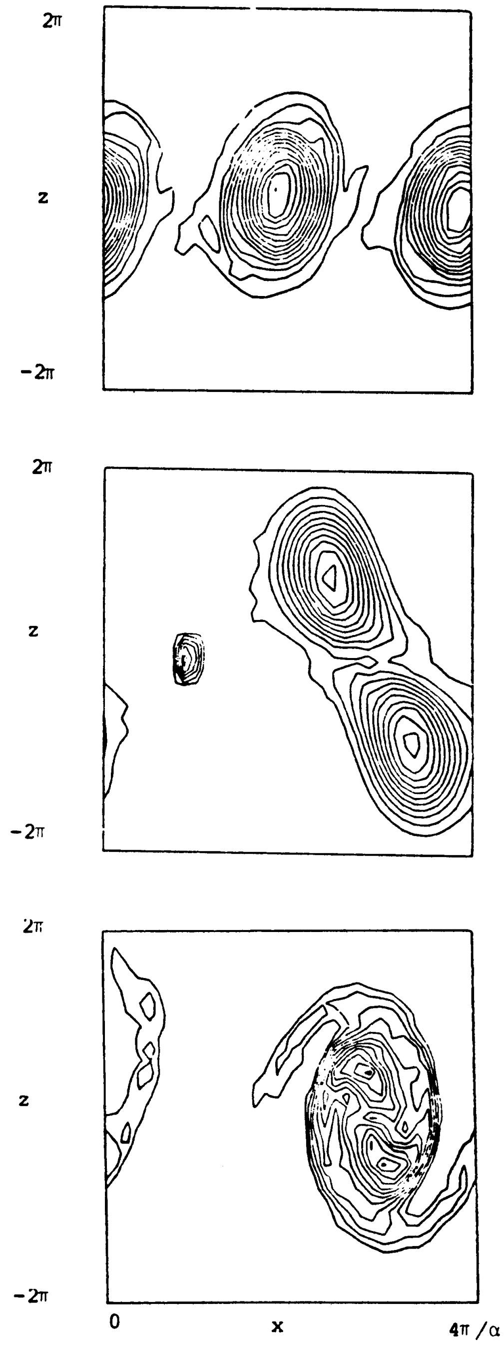

Figure 4.

Spanwise vorticity contours at $t = 48,\ 72,\ 96$ during a vortex pairing run with $R = 200$, $V_0(z) = \tanh z$, $A_{10} = 0.25$, $A_{\frac{1}{2},0} = 3 \times 10^{-5}$, $M = 16$, $N = 1$, $P = 32$, (resolution $32 \times 1 \times 32$) $\alpha = 0.43$, $\Delta t = 0.01$.

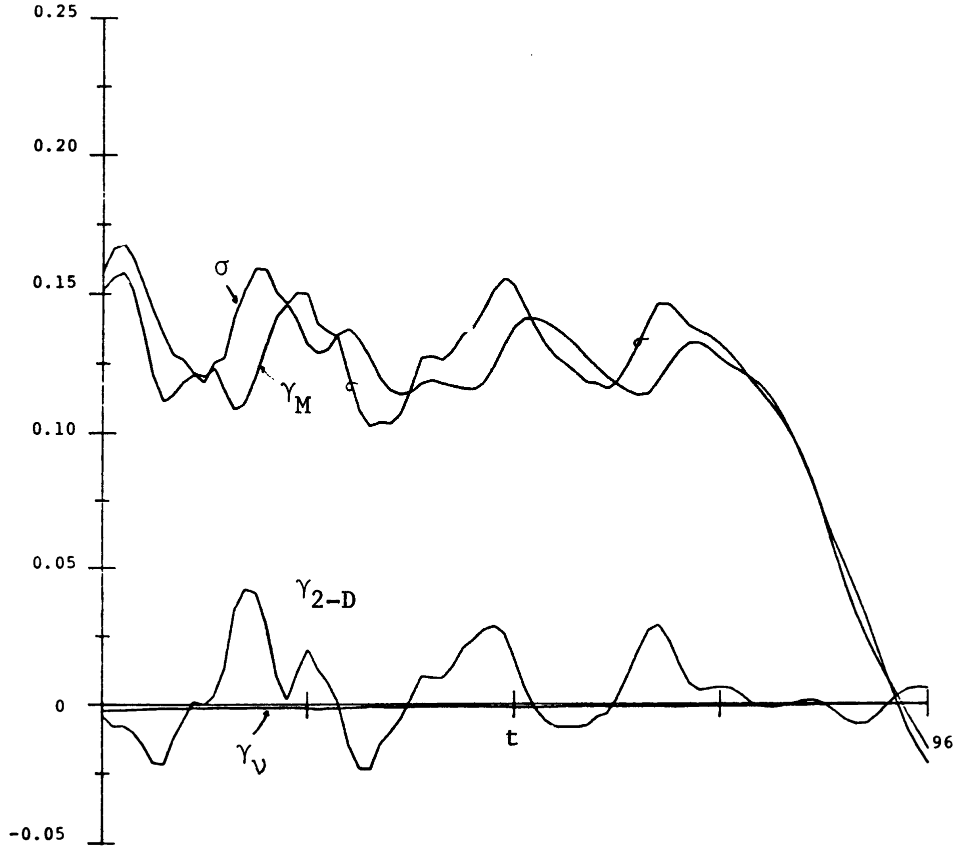

Figure 5.

A plot of the components γ_M, γ_{2-D}, γ_ν [see (3.4)] of the growth rate $\sigma_{\frac{1}{2},0}$ of pairing mode amplitude as functions of time for the same run as in Figure 4.

obtained by Kelly (1967) using perturbation theory, they differ in some important respects. First, we observe nothing very special about the 'resonant' wavenumber $\alpha \approx 0.44$ of maximum linear growth presumably because our study is a temporal, not spatial, stability analysis. Second, we do not find that the growth rate of the pairing mode is significantly enhanced by the finite-amplitude primary mode (Pierrehumbert & Widnall 1982). On the contrary, the growth rate of the pairing mode at $1/2\alpha = 0.22$ seems to be slightly less when the primary achieves finite amplitude than for the parallel shear flow.

The saturated two-dimensional flow is also subject to three-dimensional instabilities. While the laminar mean flow is inviscidly unstable only for $\alpha^2 + \beta^2 < 1$, the finite-amplitude two-dimensional flow can be unstable for large β at high R. In Fig. 6, we plot the evolution of three-dimensional disturbance energy

$$E_{3D} = \sum_m E_{m1}(t) \tag{3.5}$$

for runs with initial conditions (3.1) with $A_{10} = 0.25$, $A_{1/2,0} = 0$, $A_{11} = 10^{-6}$ with $\alpha = 0.4$, $2 \leq \beta \leq 8$. For these parameter values, the mean flow tanh z is both viscously and inviscidly stable at these three dimensional scales. Nevertheless, the saturated two-dimensional disturbed flow is strongly unstable at these scales, with disturbances growing at roughly the same rate as the inviscid two-dimensional primary instability. Since the two-dimensional modes saturate, the three-dimensional modes can achieve finite amplitudes on convective time scales and thereby modify significantly the later evolution of the flow.

The growing three-dimensional wave is localized in space on top of the two-dimensional vortex motion. In Fig. 7, a plot is given of contours of the spanwise (three-dimensional) perturbation velocity $v(x,0,z,t)$, as well as a wind plot of the finite amplitude two-dimensional flow $(u(x,0,z,t), w(x,0,z,t))$. The structure of this three-dimensional mode is not dissimilar to that found in wall-bounded flow (see Orszag & Patera 1983 for a detailed discussion of these latter modes).

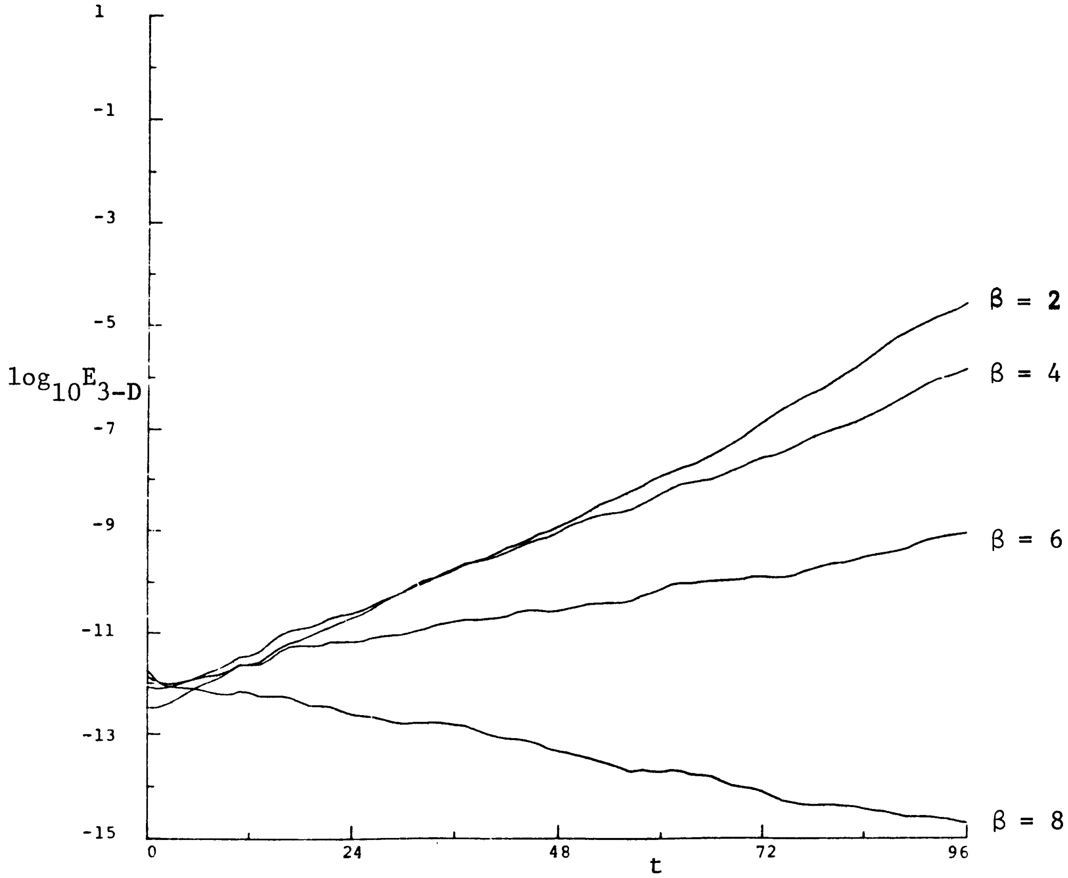

Figure 6.

A plot of the evolution of the three-dimensional disturbance energy $E_{3-D}(t)$ vs t for runs with R = 400, $U_0(z)$ = tanh z, M = 8, N = 4, P = 32 (resolution 8 x 4 x 32) α = 0.4, Δt = 0.02, A_{10} = 0.25, A_{11} = 10^{-6}, and β = 2, 4, 6, 8.

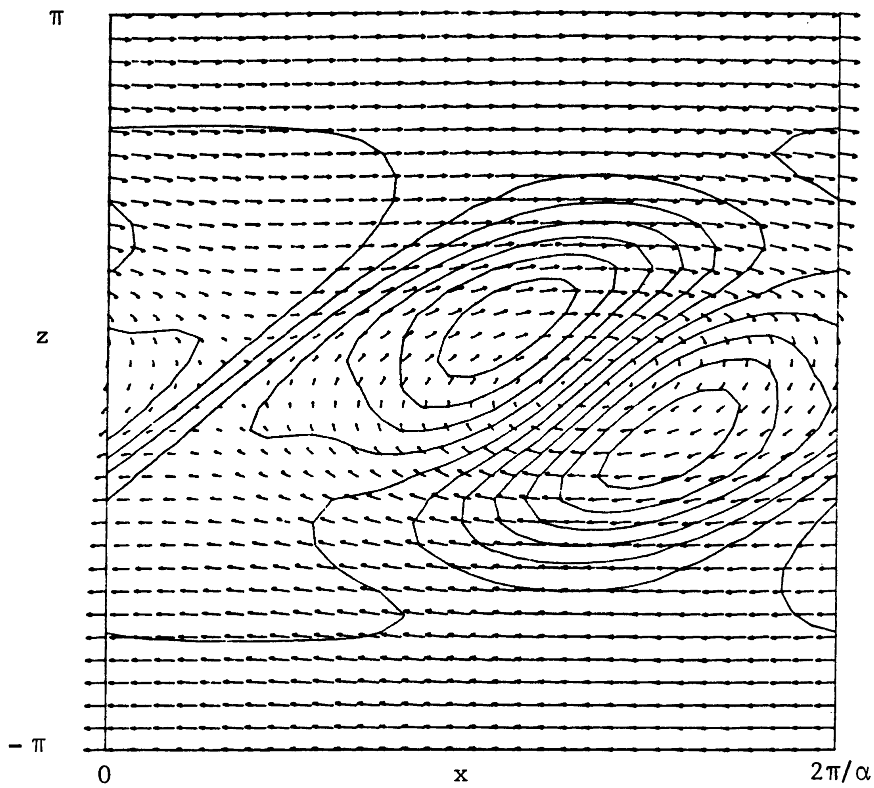

Figure 7.

Contour plot of the perturbation three-dimensional velocity component $v(x,0,z,t)$, in the plane $y = 0$ superimposed on a wind (vector) plot of the finite amplitude vortex flow $(u(x,0,z,t), w(x,0,z,t))$ whose vorticity contours are plotted in Figure 2. Here $R = 200$, $\alpha = 0.8$, $\beta = 0.8$, $U_0(z) = \tanh z$, $M = N = P = 32$ (resolution 32 x 32 x 32 with no pairing modes) and the contours are plotted at $t = 24$.

In Fig. 8, a plot of the average three-dimensional growth rate σ_{3-D} vs. β is given for various R when α = 0.4. It is apparent from the results plotted in Fig. 8 that, as R increases, σ_{3-D} approaches a finite limit for fixed β (so the secondary instability discussed is inviscid in character) and that the instability turns off for $\beta > \beta_{crit} \sim 1/3\sqrt{R}$.

The cutoff β_{crit} is due to viscous damping as nonlinear transfers vary little with β. This point is established in Fig. 10 where we plot the contributions to the growth rate σ_{3-D},

$$\frac{1}{2E_{3-D}} \cdot \frac{dE_{3-D}}{dt} \equiv \sigma_{3-D} = \gamma_M + \gamma_{2-D} + \gamma_\nu \qquad (3.6)$$

where γ_M involves the nonlinear interaction of the three-dimensional and mean flows, γ_{2-D} the interaction of the three-dimensional and two-dimensional disturbances, and γ_ν the viscous dissipation of three-dimensional energy. It is apparent from Fig. 10a that, for $\beta << \beta_{crit}$, γ_ν, $\gamma_{2-D} << \gamma_M$ so the three-dimensional modes derives its energy from the mean flow with the two-dimensional disturbance acting as a catalyst for this transfer.

On the other hand, the results plotted in Fig. 10b show that when $\beta \sim \beta_{crit}$, γ_ν is quite significant. The three-dimensional instability seems to be turned off at large cross-stream wavenumber β by increasing dissipation rather than by any significant qualitative change in nonlinear transfers from the mean and two-dimensional components.

The flows that develop from the three-dimensional secondary instability do not saturate in ordered states like those of the primary two-dimensional and pairing instabilities. Instead, the three-dimensional modes seem to lead to chaos and, finally, turbulence. In Figs. 11, contour plots of spanwise vorticity and wind plots in three-dimensional mixing layer runs (at resolution M = N = P = 32) are given at t = 36 after the three-dimensional fluctuations

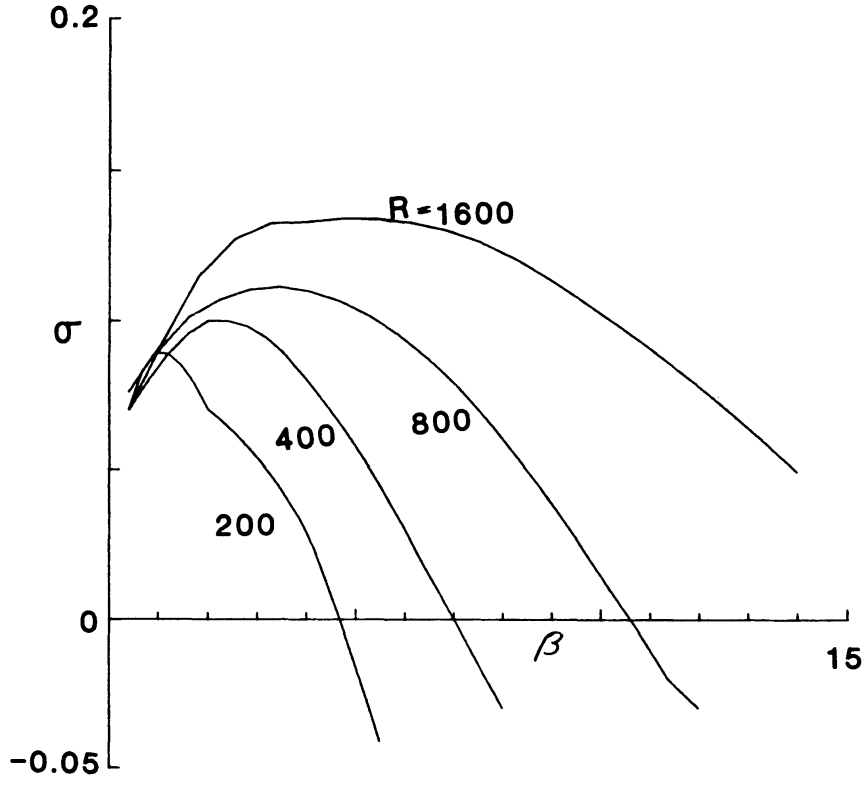

Figure 8.

A plot of the computed three-dimensional growth rate σ_{3-D} [see (3.6)] as a function of spanwise wavenumber β for various Reynolds numbers for $U_0(z) = \tanh z$. Here $\alpha = 0.4$.

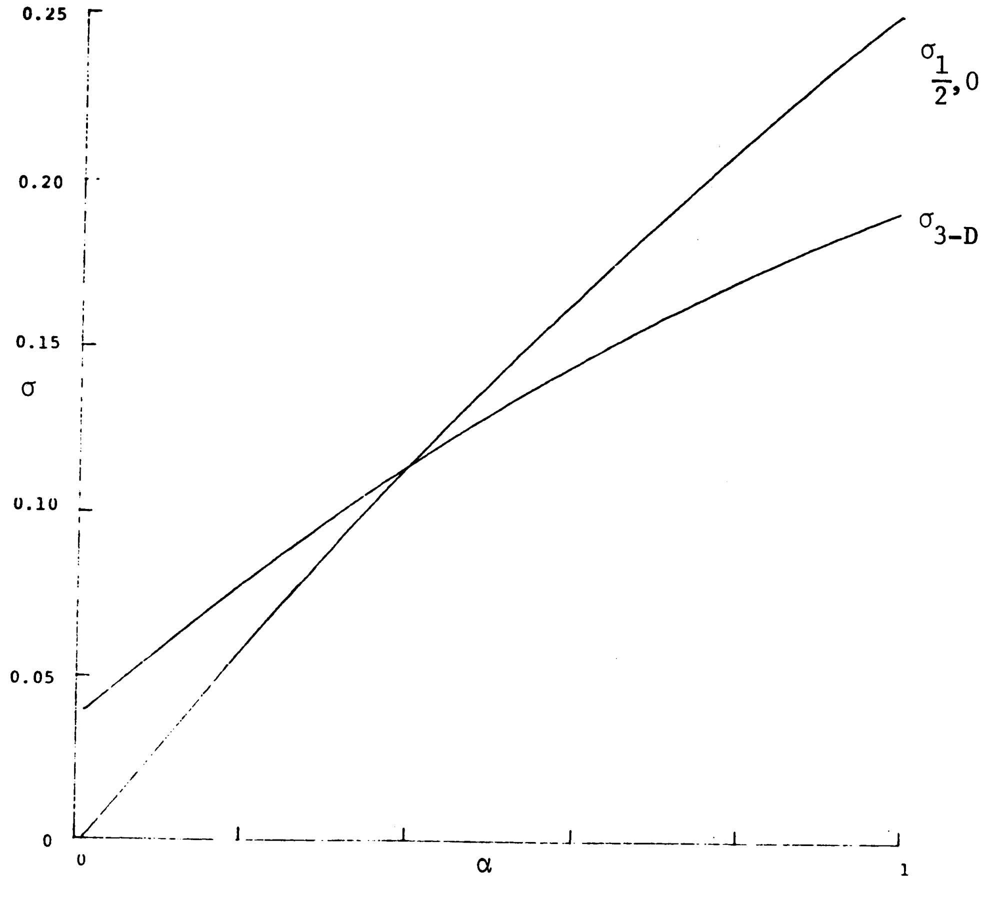

Figure 9.

A plot of the computed pairing growth rate $\sigma_{\frac{1}{2},0}$ and three-dimensional growth rate σ_{3-D} as a function of α at $R = 400$, $\beta = 0.8$ with $U_0(z) = \tanh z$. (Note that the wavenumber of the pairing mode is $\frac{1}{2}\alpha$)

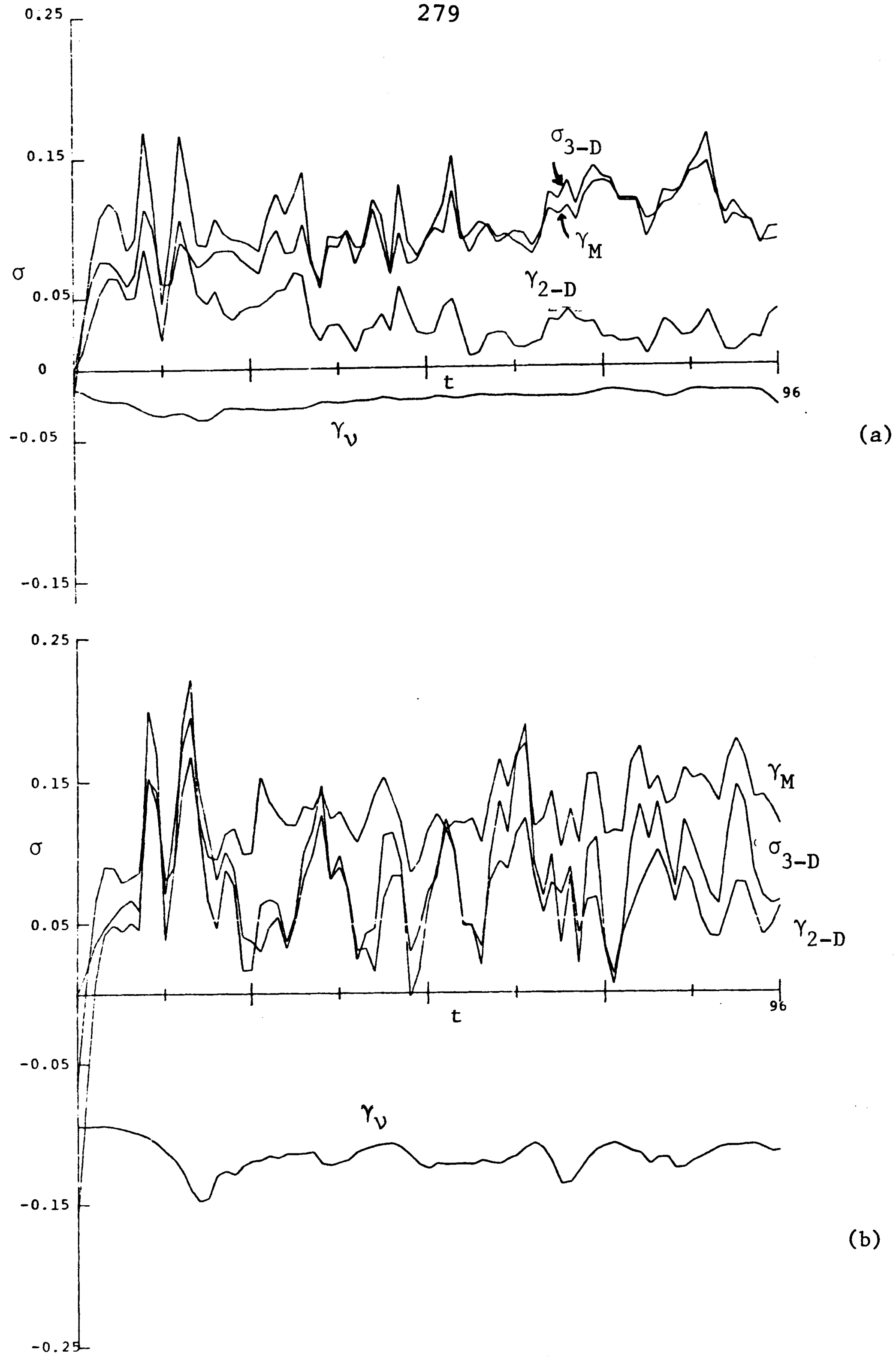

Figure 10.

A plot of the components γ_M, γ_{2-D}, γ_ν [see (3.6)] of the three dimensional growth rate σ_{3-D} as functions of time for R=400, α = 0.4, A_{10} = 0.25, A_{11} = 10^{-6}. (a) β = 4 (b) β = 6

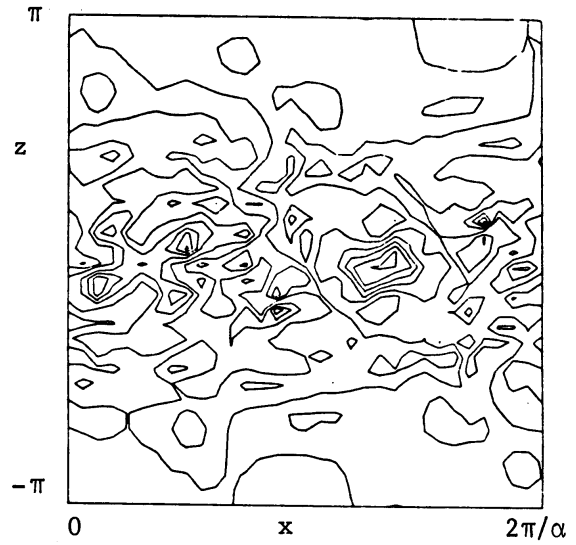

(a)

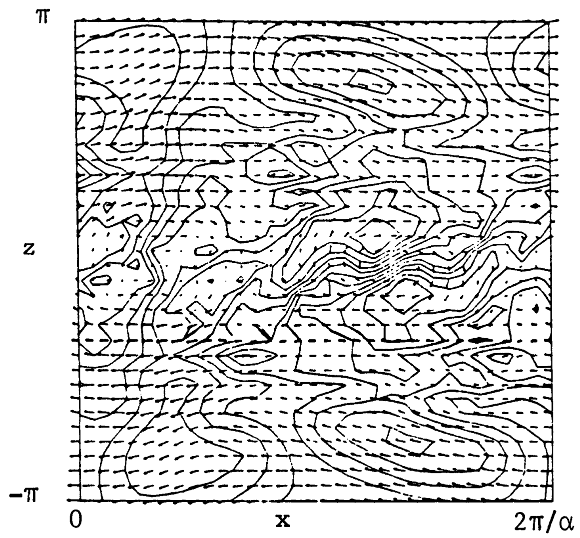

(b)

Figure 11.

(a) Contour plot of spanwise vorticity in the plane y = 0 at t = 36 for the run described in the caption to Figure 7. (b) Contours of spanwise velocity v and wind plot of (u,w) vector field in the plane y = 0 at t = 36.

become comparable to the two-dimensional amplitudes. The order apparent in Fig. 7 is partially obliterated by the three-dimensional excitations apparent in Fig. 11, but two-dimensional structure is still significant.

The nature of the competition between two-dimensional pairing and three-dimensional instability is further illustrated by the results plotted in Figs. 12, 13. In both figures, results of runs with $R = 400$, $\alpha = 0.4$, $\beta = 0.2$ are plotted. In Fig. 12, the initial conditions are chosen so that the pairing mode perturbation is much larger than that of the three-dimensional perturbation; it seems that the pairing process slightly inhibits the three-dimensional instability. In Fig. 13, the evolution of the instabilities are plotted when the initial three-dimensional perturbation is much larger than the pairing mode. In this case, it seems that the pairing instability is nearly unaffected by the three-dimensional instability before finite amplitudes are reached; when the three-dimensional mode becomes finite amplitude, the flow is chaotic so a higher resolution three-dimensional code should be used to study the energetics.

5. Discussion

The principal result of this paper is the demonstration that small-scale three-dimensional instabilities like those previously studied by Orszag & Patera (1980, 1981, 1982), Pierrehumbert & Widnall (1982) exist in viscous free shear flows and that these instabilities persist to moderately low Reynolds number. It is possible that these modes are responsible for the initial development of three dimensionality in these shear flows. The dynamics of the three-dimensional instability is qualitatively the same as that of the three-dimensional instabilities studied by us in wall-bounded shear flows. In particular, the instability does not appear to be similar to the Görtler instability in curved channels, as the instability has significant streamwise variation along the two-dimensional eddy. While the instability shares some features of a classical inflectional instability, including phase locking with the primary vortex, inflectional instability is preferentially

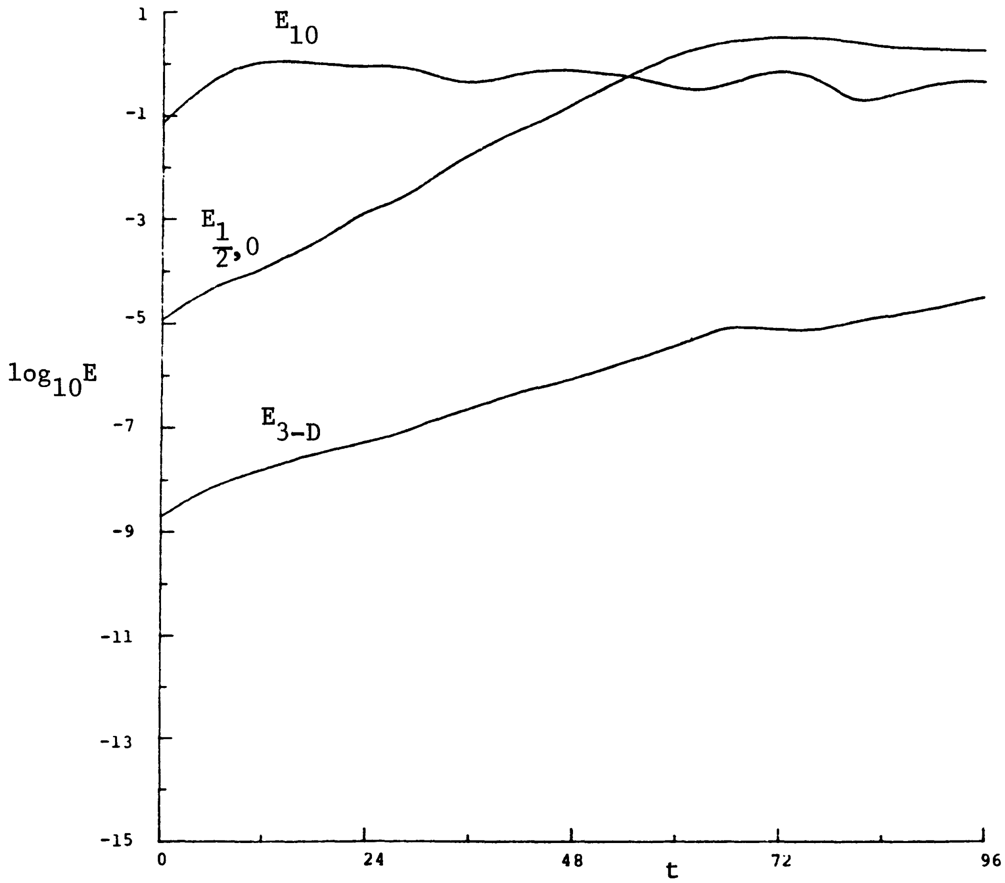

Figure 12.

A plot of the evolution of the energies E_{10}, $E_{\frac{1}{2},0}$, E_{3-D} vs t for a run with R = 400, $U_0(z)$ = tanh z, α = 0.4, β = 0.2, M = 8, N = 4, P = 32, and initial conditions A_{10} = 0.25, $A_{\frac{1}{2},0}$ = 4 x 10^{-3}, A_{11} = 3.3 x 10^{-5}. The subharmonic pairing mode dominates the three-dimensional mode.

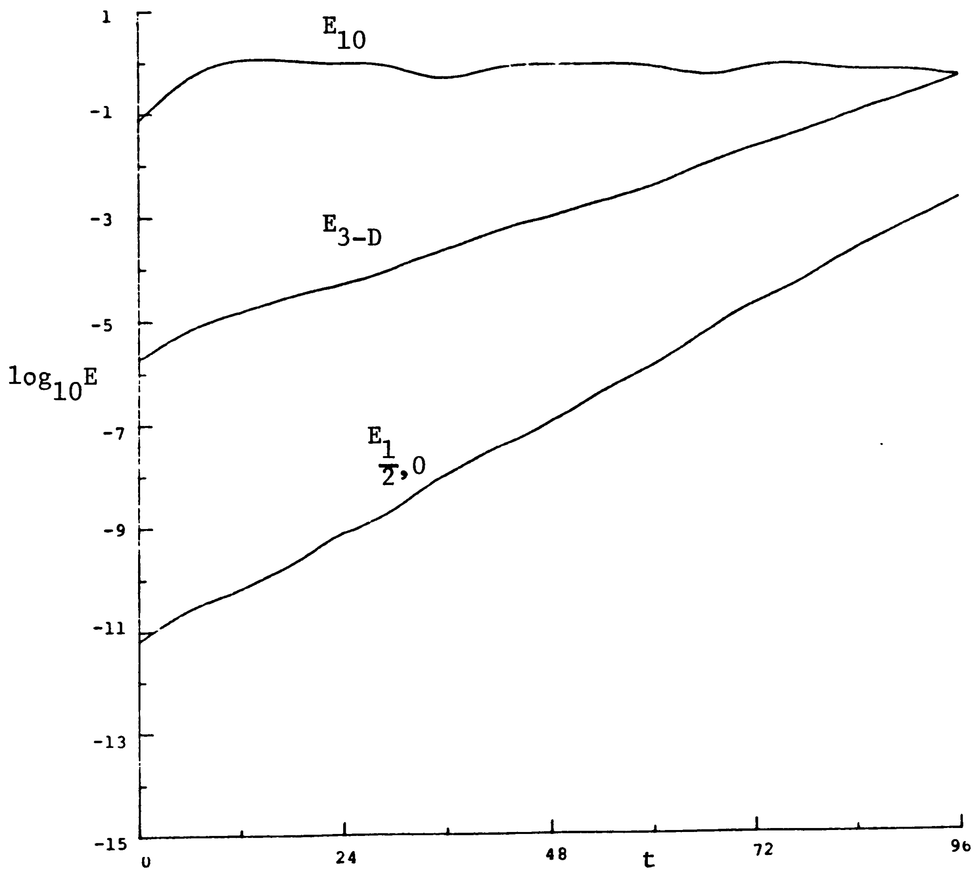

Figure 13.

Same as Figure 12, except that the initial conditions are $A_{10} = 0.25$, $A_{\frac{1}{2},0} = 3 \times 10^{-6}$, $A_{11} = 10^{-3}$. The three-dimensional mode initially dominates the pairing mode.

two-dimensional but the present instability is not.

It seems that the mechanics of transition in the free shear flows studied here may, in a sense, be rather more complicated than in the case of wall-bounded shear flows. In the latter case, linear instabilities are often viscously driven and, therefore, weak, so they can not be directly responsible for the rapid distortions characteristic of transition. On the other hand, free shear flows are subject to a variety of inviscid instabilities so there may be many paths to turbulence. The choice of which path is taken in any individual flow may depend on the results of competition between priamry, subharmonic, and three-dimensional instabilities, all of which are convectively driven and, therefore, strong with comparable growth rates. Thus, it may be that the evolution of free-shear flows in transitional regimes may depend significantly on the past history of the flow, including the mechanism of its generation and the external environment in which the flow is embedded.

This work was supported by the Office of Naval Research under Contract N00014-82-C-0451, the National Science Foundation under Grant ATM84-14410, and the Air Force Office of Scientific Research under Contract F49620-85-C-0026. The computations reported here were performed at the Computing Facility of the National Center for Atmospheric Research, Boulder, CO, which is supported by the National Science Foundation.

References

Bernal, L.P., Breidenthal, R.E., Brown, G.L., Konrad, J.H., & Roshko, A. 1979 On the development of three dimensional small scales in turbulent mixing layers. In Proc. 2nd Int. Symp. on Turbulent Shear Flows, Imperial College, London.

Brachet, M.E., Meiron, D. I., Orszag, S.A., Nickel, B.G., Morf, R.H. & Frisch, U. 1983 Small Scale structure of the Taylor-Green vortex. J. Fluid Mech., 130, 411-452.

Browand, F.K. & Troutt, T., 1980 A note on spanwise structure in the two-dimensional mixing layer. J. Fluid Mech. 97, 771.

Brown, G.L. & Roshko, A. 1974 On density effects and large structures in turbulent mixing layers. J. Fluid Mech. 64, 775.

Collins, D.A. 1982 A numerical study of the stability of a stratified mixing layer. Ph.D. Thesis, Department of Mathematics, McGill Univ., Montreal.

Deville, M. O., Israeli, M. & Orszag, S.A. 1983 Splitting methods for incompressible flow problems. To be published.

Drazin, P.G. & Reid, W.H. 1981 Hydrodynamic Stability, Cambridge University Press.

Ho, C.M. & Huang, L.S. 1982 Subharmonics and vortex merging in mixing layers. J. Fluid Mech. 119, 443-473.

Miksad, R.W. 1972 Experiments on the nonlinear stages of free shear layer transition. J. Fluid Mech. 56, 645.

Orszag, S.A. & Patera, A.T. 1980 Subcritical transition to turbulence in plane channel flows. Phys. Rev. Lett. 45, 989.

Orszag, S.A. & Patera, A.T. 1981 Subcritical transition to turbulence in planar shear flows. In Transition and Turbulence (ed. R.E. Meyer), Academic, New York.

Orszag, S.A. & Patera A.T. 1983 Secondary instability of wall-bounded shear flows. J. Fluid Mech., in press.

Patnaik, P.C., Sherman, F.S. & Corcos, G.M. 1976 A numerical simulation of Kelvin-Helmholtz waves of finite amplitude. J. Fluid Mech. 73, 215.

Pierrehumbert, R.T. & Widnalll, S.E. 1982 The two- and three-dimensional instabilities of a spatially periodic shear layer. J. Fluid Mech. 114, 59.

Riley, J.J. & Metcalfe, R.W. 1980 Direct numerical simulation of a perturbed, turbulent mixing layer. AIAA Paper No. 80-0274.

Stuart, J.T. 1967 On finite amplitude oscillations in laminar mixing layers. J. Fluid Mech. 29, 417.

Winant, C.D. & Browand, F.K. 1974 Vortex pairing: the mechanism of turbulent mixing-layer growth at moderate Reynolds number. J. Fluid Mech. 63, 237.

Wygnanski, I. Oster, D., Fiedler, H. & Dziomba, B. 1979 On the perservance of quasi-two-dimensional eddy-structure in a turbulent mixing layer. J. Fluid Mech. 93, 325.